SCI. MAR., 65 (Suppl. 1): 187-194 SCIENTIA MARINA 2001

AN INTERDISCIPLINARY VIEW OF THE OCEAN. *J.L. PELEGRÍ, I. ALONSO and J. ARÍSTEGUI (eds.)*

# Sensitivity of an idealised subtropical gyre to the eastern boundary conditions*

I. LÁIZ, P. SANGRÀ, J.L. PELEGRÍ, and A. MARRERO-DÍAZ

Departamento de Física, Facultad de Ciencias del Mar, Universidad de Las Palmas de Gran Canaria, Canary Islands, Spain.

SUMMARY: The flow pattern of the North Atlantic Subtropical Gyre (NASG) is simulated using a highly idealised one-layer quasi-geostrophic wind-driven model. The novel feature of the model is the specification of the eastern boundary conditions. This is an upwelling favourable region with a quasi-permanent southward flowing coastal jet, which is fed by the eastern branch of the Canary Current. The corresponding boundary conditions are non-zero normal flux and constant potential vorticity, the latter being consistent with the generation of anticyclonic vorticity by the coastal jet. We examine the sensitivity of the model to the eastern boundary conditions and compare the results with recent observations for the region.

*Key words*: numerical modelling, subtropical gyre, eastern boundary conditions, Canary Current.

## INTRODUCTION

The eastern region of the North Atlantic Subtropical Gyre (NASG) shows an anticyclonic loop formed by the Azores Current (AC), the Canary Current (CC), and the North Equatorial Current (NEC). The AC progressively turns to the south and southwest into the CC, before leaving the region towards the west as the NEC (Fig. 1a, reproduced from Stramma, 1984). The total amount of water that transits the region is about 12 Sv (Stramma, 1984; Siedler and Onken, 1996). North of 30ºN and off the African continental platform there is permanent onshore geostrophic transport of about 1-2 Sv. This water flux necessarily recirculates south close to the coast until it rejoins the interior deep ocean between 20 and 25ºN (Stramma, 1984; Stramma and Siedler, 1988), in what we may call the eastern branch of the CC. This eastern branch is so narrow that it does not show up in Stramma (1984) and Stramma and Siedler (1988) maps, which where obtained from deep ocean data. Arhan *et al*. (1994), however, have inferred an eastward transport of about 11 Sv into the eastern boundary layer and at densities lower than 27.25 sigma-theta, which appears to feed southward alongshore currents.

One could be tempted to associate the permanent eastern branch with the baroclinic coastal upwelling jet that develops in any upwelling region (Pelegrí *et al*., 1997). This may be partially true but a difficulty with this interpretation is that north of 30ºN upwelling does not take place during winter. This suggests that the mechanism of coupling between the interior and coastal oceans is not simply forced by coastal upwelling but is a complex process requiring careful analysis.

Data collected during the CANIGO project have improved the knowledge of the Canary Current area. Some of these measurements have been made very near to the continental platform and

*Received February 11, 2000. Accepted August 28, 2000.

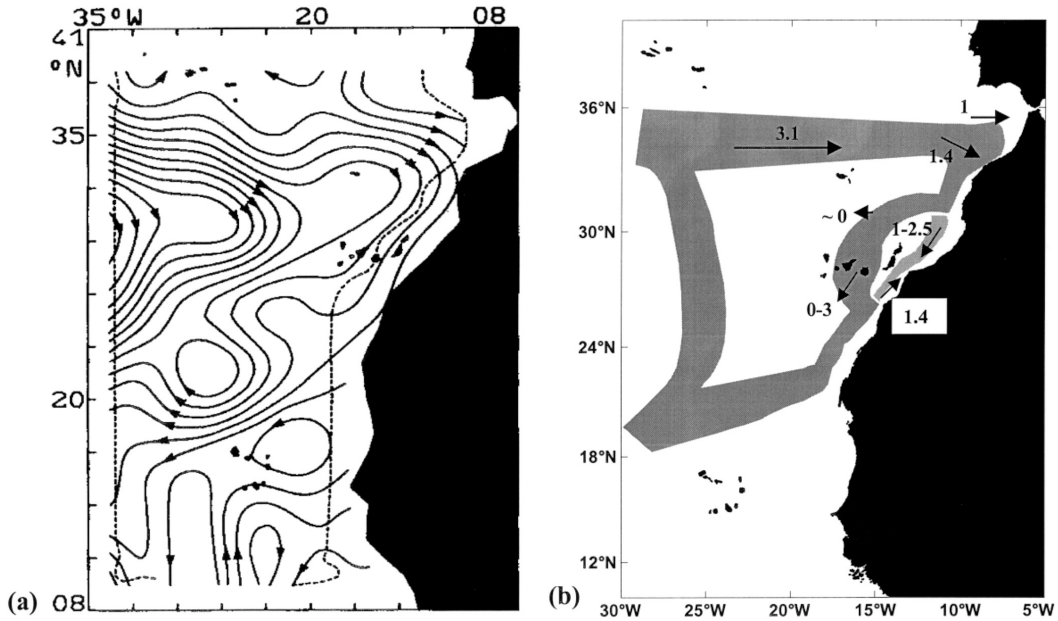


FIG. 1. – (a) Mean annual circulation streamlines for the upper 800 m according to Stramma (1984); each flow line represents 1 Sv. (b) Schematic mean water transport (in Sv) as obtained from two years of quarterly XBT data along the transects shown.

confirm that the recirculation of the eastern branch of the CC takes place in a very narrow region (Pelegrí *et al.*, 1999). They have shown that this water flux sometimes continues southward between the Canary Islands and the African coast, but at other times it appears to rejoin the interior ocean at Cape Ghir before flowing south through the Canary Archipelago (Fig. 1b).

The aim of this study is to examine how the coastal ocean may drive the eastern branch of the CC. For this purpose we use a very simple one-layer quasigeostrophic model driven by idealised zonal winds, and modify the eastern boundary conditions to simulate the effect of the coastal ocean. The main point is that the water in the coastal region moves southwards, breaking lines of constant planetary vorticity along a meridional band of constant potential vorticity. We will see that this gives rise to anticyclonic vorticity at the boundary, which may be interpreted as being generated by the coastal jet. This condition, together with the possibility of non-zero normal flux, produces rather realistic simulations of the easternmost branch of the CC.

## THE ONE-LAYER QUASIGEOSTROPHIC MODEL

A simple quasigeostrophic one-layer model is used to represent the circulation pattern of the NASG. The ocean basin is idealised as a rectangular basin with a flat bottom and constant depth $D$ on a mid-latitude β-plane. It lies in the 77-15ºW longitude and 10-40ºN latitude bands. We have assumed a homogeneous and incompressible fluid subject to a zonal, steady, anticyclonic single-gyre wind stress pattern. The model was formulated using the quasi-geostrophic barotropic vorticity equation (Pedlosky, 1979):

$$\frac{\partial \zeta}{\partial t} + J(\psi,\zeta) + \beta_0 v = \\ = \frac{1}{D}\hat{k}\cdot curl\,\frac{\vec{\tau}}{\rho_0} - \frac{f_0}{D}\frac{\delta_E}{2}\zeta + A_h\nabla^2\zeta \qquad (1)$$

and the Poisson equation:

$$\zeta = \nabla^2\psi \qquad (2)$$

where $\zeta$ is the relative vorticity and $\psi$ the stream function, $J(\psi,\zeta)$ is the Jacobian, $D$ is the water depth, $\vec{\tau} = (\tau_x, \tau_y, 0)$ the surface wind stress, $\rho_0$ the mean density of water, $\delta_E = (2A_v / f_0)^{1/2}$ the Ekman layer thickness, $r = f_0\,\delta_E / 2D$ the bottom friction coefficient, and $A_h$ the horizontal diffusion coefficient.

The wind stress and its curl have the form

$$\tau_x = -\tau_0 \cos\left(\frac{\pi y}{L}\right), \quad \tau_y = 0,$$

$$curl\ \vec{\tau} = -\frac{\pi\tau_0}{L} sin\left(\frac{\pi y}{L}\right).$$

The non-dimensionalisation was performed by scaling: $(x, y) = L(x', y')$, $(u, v) = U(u', v')$, $\zeta = (U/L)\zeta'$ , $\tau_x = \tau_0 \tau'$, and $t = (1/\beta_0 L)t'$, where the primes indicate non-dimensional variables (Pedlosky, 1979). Thus, the non-dimensional vorticity equation becomes:

$$\frac{\partial \zeta'}{\partial t'} + \varepsilon J(\psi', \zeta') + v' =$$
$$= -\alpha \ \ sin(\pi y') - \mu \zeta' + E\nabla^2 \zeta'$$

where the non-dimensional parameters are the Rossby number $\varepsilon = U/(\beta_0 L^2)$, the non-dimensional bottom friction coefficient $\mu = r/(\beta_0 L)$, the wind forcing coefficient $\alpha = (\tau_0 \pi)/(\rho_0 DL\beta_0 U)$, and the horizontal Ekman number $E = (\delta_M / L)^3$; the Munk boundary layer scale is defined as $\delta_M \equiv (A_h / \beta_0)^{1/3}$.

In order to solve the vorticity and continuity equations we need to specify boundary conditions for both the vorticity and the stream function. The standard boundary conditions are no-slip at the meridional boundaries, slip at the zonal boundaries, and no-normal flux at all boundaries (Case 1, Table 1); a slightly different possibility is to use a slip condition at the eastern boundary (Case 2, Table 1). These boundary conditions are specified as follows (Roache, 1982):

$$\psi_b = 0, \ \ no\text{-}normal\ flux$$

$$\zeta_b = 0, \ \ slip$$

$$\zeta_b = \frac{\partial^2 \psi_b}{\partial n^2} \ , \ \ no\text{-}slip$$

where the subscript $b$ indicates the grid point at the boundary and n is the direction normal to the wall. The finite difference expression for the no-slip condition (first order form)

$$\zeta_b = \frac{2(\psi_{b-1} + \psi_b)}{\Delta n^2} \ , \ \ no\text{-}slip \text{ (first order form)}$$

where $\Delta n$ is the distance, normal to the wall, from grid point ($b$-1) to grid point ($b$).

One alternative to the above standard boundary conditions is as follows. First, we may replace the no-normal flux condition by a condition that allows a coastward flux across the eastern boundary, that is,

$$\psi_e = \psi_{e\text{-}1} \ , \ \ non\text{-}zero\ normal\ flux$$

where the subscript $e$ indicates the grid point at the eastern boundary. Taking into account that our eastern boundary corresponds to the 15ºW parallel, the non-zero flux condition will allow the outflow of interior water into the near-coastal region and its reappearance further south (see Fig. 1a).

TABLE 1. – Eastern boundary conditions employed in the main numerical simulations.

| Case | Stream function | Vorticity |
|---|---|---|
| 1 | zero normal flux | no-slip |
| 2 | zero normal flux | slip |
| 3 | non-zero normal flux 20-40ºN<br>zero normal flux 10-20ºN | no-slip |
| 4 | non-zero normal flux 20-40ºN<br>zero normal flux 10-20ºN | slip |
| 5 | non-zero normal flux 20-40ºN<br>zero normal flux 10-20ºN | constant $q$ 20-40ºN<br>no-slip 10-20ºN |
| 6 | non-zero normal flux 20-40ºN<br>zero normal flux 10-20ºN | constant $q$ 20-40ºN<br>slip 10-20ºN |
| 7 | non-zero normal flux 32-40ºN<br>zero normal flux 27-32ºN<br>non-zero normal flux 20-27ºN<br>zero normal flux 10-20ºN | <br><br>constant $q$ 20-40ºN<br>no-slip 10-20ºN |
| 8 | non-zero normal flux 32-40ºN<br>zero normal flux 27-32ºN<br>non-zero normal flux 20-27ºN<br>zero normal flux 10-20ºN | <br><br>constant $q$ 20-40ºN<br>slip 10-20ºN |
| 9 | non-zero normal flux 32-40ºN<br>zero normal flux 27-32ºN<br>non-zero normal flux 20-27ºN<br>zero normal flux 10-20ºN | constant $q$ 32-40ºN<br>no-slip 27-32ºN<br>constant $q$ 20-27ºN<br>no-slip 10-20ºN |
| 10 | non-zero normal flux 32-40ºN<br>zero normal flux 27-32ºN<br>non-zero normal flux 20-27ºN<br>zero normal flux 10-20ºN | constant $q$ 32-40ºN<br>slip 27-32ºN<br>constant $q$ 20-27ºN<br>slip 10-20ºN |
| 11 | non-zero normal flux 20-40ºN<br>zero normal flux 10-20ºN | constant $q$ 32-40ºN<br>no-slip 27-32ºN<br>constant $q$ 20-27ºN<br>no-slip 10-20ºN |
| 12 | non-zero normal flux 20-40ºN<br>zero normal flux 10-20ºN | constant $q$ 32-40ºN<br>slip 27-32ºN<br>constant $q$ 20-27ºN<br>slip 10-20ºN |

Second, we may modify the slip/no-slip conditions through the specification of a meridional band of constant potential vorticity, which would allow southward flux, by requiring:

$$q_e = \frac{\zeta_e + f_e}{D} = const.$$

As the basin has constant depth, this is equivalent to $\zeta_e + f_e = const.$ On a mid-latitude $\beta$-plane, the Coriolis parameter is expressed as: $f = f_0 + \beta_0 y$ . Taking this into account, the relative vorticity along the eastern boundary takes the form:

$$\zeta_e = \beta_0 (y_c - y) - \frac{2(\psi_{e-1} + \psi_e)}{\Delta n^2} \ ,$$
$$y \in [\, y_c, y_N], \quad constant\ potential\ vorticity$$

where $y_c$ is the separation latitude and $y_N$ is the northern limit of the basin. This is the general form of this condition, considering the no-slip condition at the eastern boundary between $y = 0$ and $y = y_c$. Notice that $\psi_e = 0$ when the standard condition of no-normal flux is considered at latitudes between $y = y_c$ and $y = y_N$. We may notice that this condition involves the generation of anticyclonic vorticity at the eastern boundary, as if it were induced by the horizontal shear produced by the intense coastal jet.

The alternative set of boundary conditions, or any combination between them and the original ones, are theoretically reasonable. Our purpose here is to examine how they modify the numerical results and which modification bears the closest resemblance to the actual streamlines in the region.

The numerical integration of the equations is done using the finite-difference method. The Leapfrog scheme was used to solve the vorticity equation and a successive over-relaxation (SOR) approach was used for the Poisson equation (Roache, 1982). The Jacobian in the vorticity equation was written following Arakawa's scheme (Arakawa, 1966). We used a time lagged diffusion to reduce numerical instabilities (Roache, 1982), and an Asselin time filter (Asselin, 1972) was included to avoid instabilities induced by the Leapfrog method. A constant mesh spacing in the $x$ (longitude) and $y$ (latitude) directions was used, the spatial resolution being $\Delta x = \Delta y = 0.5^\circ$.

## TEST CASES

The standard conditions, which fully ignore the interaction of the coastal upwelling region with the interior flow, correspond to Cases 1 and 2 of our simulations (Table 1). On the other hand, the influence of the coastal ocean on the interior gyre may be assessed through a proper specification of the eastern boundary conditions as discussed above. A summary of the eastern boundary conditions used for the main test cases is presented in Table 1. This is not an exhaustive list of all possible simulations but illustrates the main cases we have considered.

Except for the standard cases (1 and 2), the eastern boundary was divided into two or four subregions. The physical justification behind the division into two subregions, one between 10 and 20ºN and the other between 20 and 40ºN, corresponds to the main circulation pattern of the eastern subtropical gyre (Fig. 1a). This pattern shows the AC and CC impinging eastward north of the Canary Islands and separating near Cape Blanc (near 20ºN) as a quasi-permanent giant filament (Gabric et al., 1993), leaving behind the so-called shadow zone (Luyten et al., 1983; Kawase and Sarmiento, 1985; Stramma, 1984; Schmitz and McCartney, 1993).

The physics behind the division into four subregions (10-20ºN, 20-27ºN, 27-32ºN, 32-40ºN) lies in the fine details of the large-scale circulation pattern and coastal upwelling regime (Fig. 1b). The 20-27ºN subregion roughly corresponds to the permanent upwelling region off northwest Africa, between Cape Blanc and Cape Bojador. In this subregion we may expect water leaving the interior ocean and feeding a southward flowing coastal jet, providing a sensible physical justification for a constant potential vorticity band. The 27-32ºN subregion roughly represents the boundary between Cape Bojador and Cape Ghir, characterised by the presence of the Canary Islands very close to the upwelling region and on the path of the southward CC. In this subregion upwelling is usually relatively weak and we could imagine that the Canary Islands may cause a perturbation to the CC. The 32-40ºN subregion roughly corresponds to the boundary region between Cape Ghir and the Strait of Gibraltar, where significant onshore geostrophic flux has been observed (Stramma, 1984; Stramma and Siedler, 1988).

All results discussed in the next section correspond to $\beta_0 = 2.25 \times 10^{-11}$ m$^{-1}$ s$^{-1}$, $A_h = 10^2$ m$^2$ s$^{-1}$, $\tau_0 = 0.1$ N m$^2$, and $D = 800$ m. The water depth was chosen to facilitate the comparison between the model results and Stramma's (1984) observations. With these values the vertical diffusion coefficient would be $A_v = 0.08$ m$^2$s$^{-1}$, the Ekman layer thickness $\delta_E = 50$ m, the Munk boundary layer $\delta_M = 16.5$ Km, and the bottom friction coefficient $r = 1.95 \times 10^{-6}$ s$^{-1}$. These last values correspond to an Ekman layer much smaller than the water depth and a time scale associated with bottom friction about 30 times larger than the rotation period. They also show that the Munk boundary layer is much smaller than the region modified by the eastern boundary conditions.

## RESULTS AND DISCUSSION

Figure 2 presents the streamlines of the whole subtropical gyre for Cases 1, 5 and 9, with each flow line corresponding to 2.5 Sv. These figures

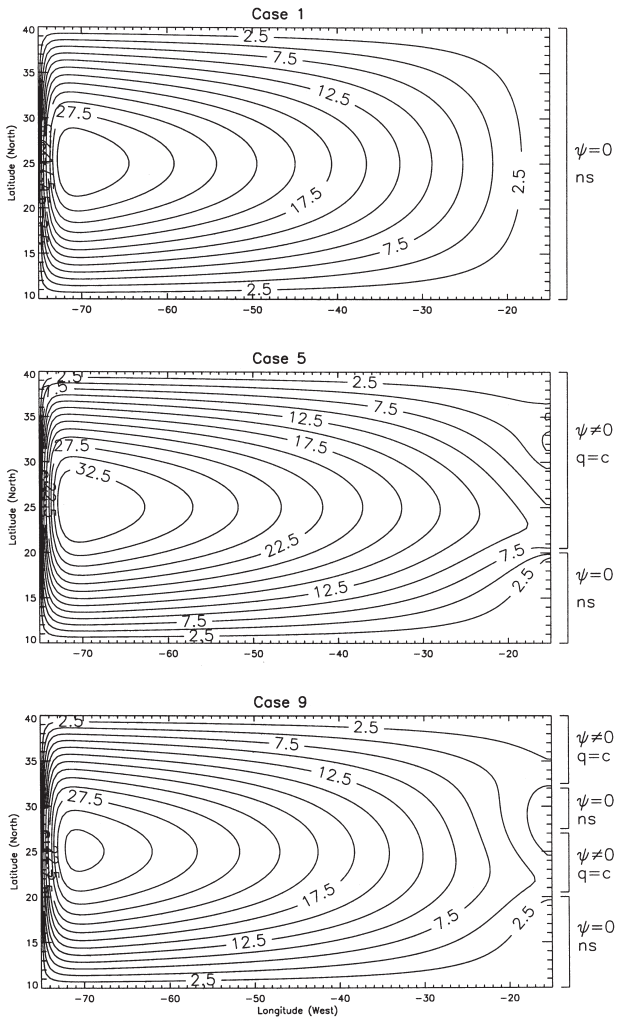


FIG. 2. – Integrated volume transport, with each flow line representing 2.5 Sv (ns: no-slip; q = c: constant potencial vorticity; $\psi = 0$: zero normal flux; $\psi \neq 0$: non-zero normal flux).

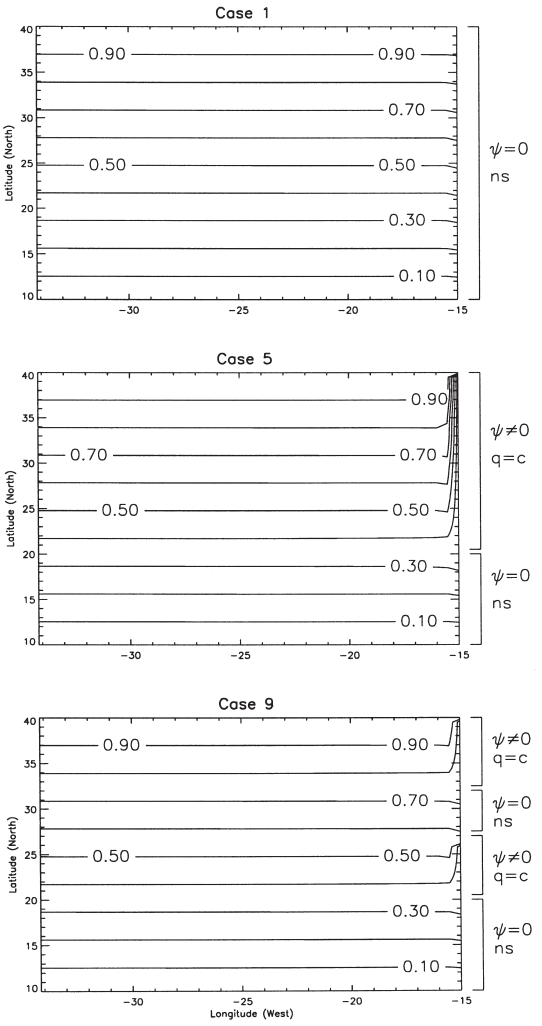


FIG. 3. – Adimensional potential vorticity (ns: no-slip; q = c: constant potencial vorticity; $\psi = 0$: zero normal flux; $\psi \neq 0$: non-zero normal flux).

clearly illustrate the influence of the eastern boundary conditions in the eastern subtropical gyre, which makes it possible to reproduce a number of observational features. Case 1 shows the stream function for the no slip and no-normal flux standard conditions at the whole eastern boundary. Case 5 (the eastern boundary is divided into two subregions) shows the drainage of about 9 Sv of interior water into the coastal region north of the Canary Archipelago and its reincorporation to the deep ocean at a latitude near Cape Blanc. This figure also illustrates the existence of two small-scale loops between 30 and 35ºN but, as it will be shown later, their existence depends on the size of the upper eastern boundary region. Case 9 (the eastern boundary is divided into four subregions) shows about 3 Sv recirculating back and forth into the coastal ocean, in a rather large loop. This figure illustrates what could be interpreted as the flow separation near Cape Ghir (at about 32ºN), its reincorporation to the coastal ocean south of the Canary Islands, and its definitive separation near Cape Blanc.

Figure 3 illustrates the potential vorticity distribution near the eastern boundary that corresponds to Cases 1, 5 and 9. In all three cases the vorticity distribution is dominated by the planetary vorticity, but Case 5 shows the existence of one meridional band of constant potential vorticity at the eastern boundary, while Case 9 includes two bands. An interesting point is that the effect of these conditions on the vorticity field is limited to a region of very small horizontal extent as compared with the modification experimented by the flow pattern. In some instances it may appear as if this small region is of the same size as the grid used for the numerical calculations (i.e. 0.5º). Using better numerical resolution, how-

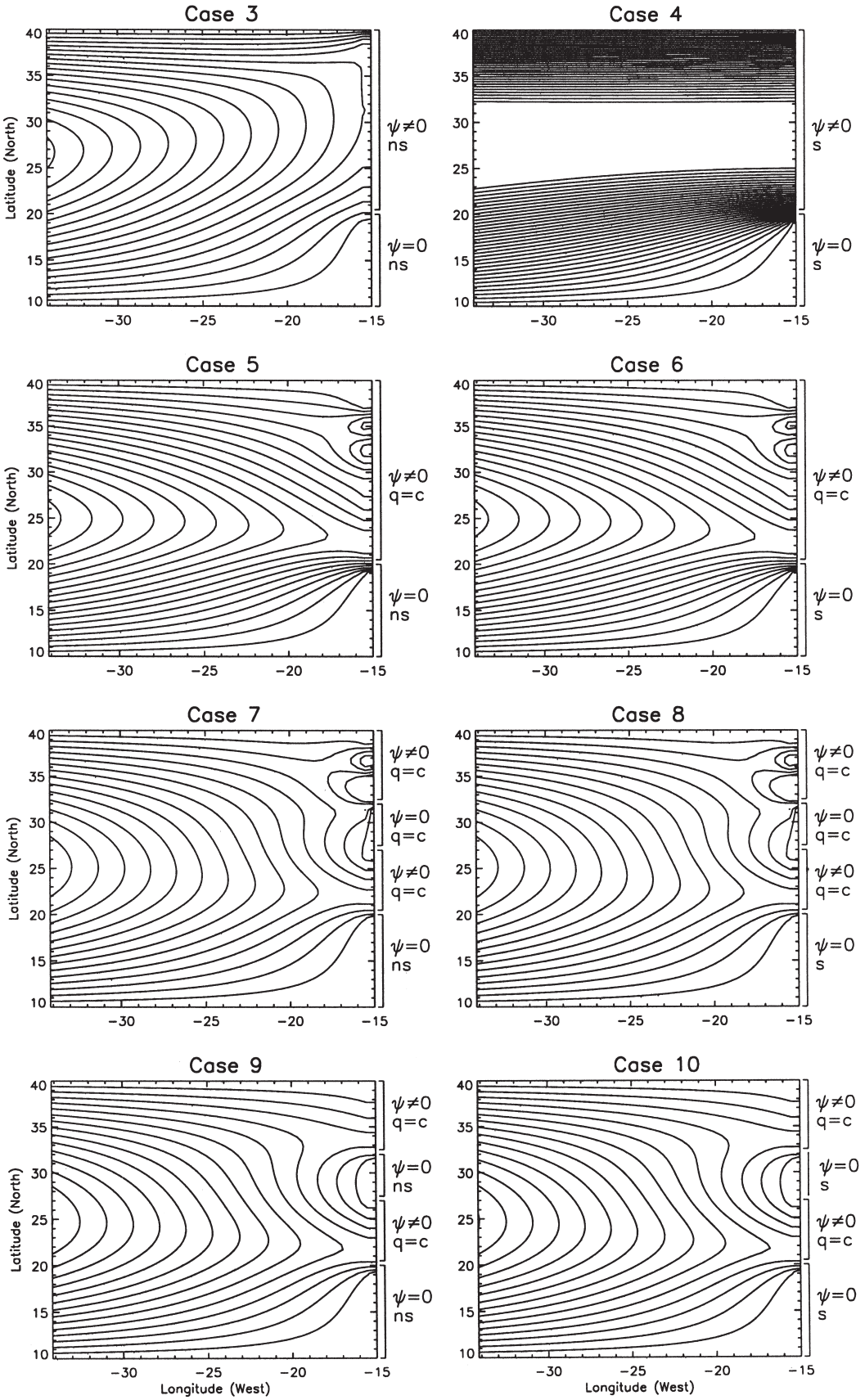


FIG. 4. – Integrated volume transport; each flow line represents 1 Sv (ns: no-slip; q = c: constant potencial vorticity; $\psi = 0$: zero normal flux; $\psi \neq 0$: non-zero normal flux).

ever, does not change the character of the solution and takes much more computational time.

The details of the results illustrated in Figures 2 and 3 depend on the wind forcing and on the meridional limits of the eastern boundary regions. The wind forcing is quite critical in controlling the amount of recirculating water in the whole subtropical gyre and particularly in the eastern branch of the eastern boundary current. In this paper we have used an idealised wind stress corresponding to a sinusoidal meridional wind variation with an amplitude of about 6 m $s^{-1}$. This appears to be a reasonable approximation, the exact wind distribution not being critical to the study of the role played by the coastal ocean in the eastern boundary circulation. We made numerical runs for several different wind stresses, resulting in different amounts of recirculating water but similar qualitative patterns. Regarding the meridional limits of the eastern boundary subregions, we performed a number of experiments which illustrate that these limits are important in controlling the small-scale patterns near the eastern boundary, but do not produce any major change in the large-scale patterns. Some of these modifications will be illustrated below.

Table 1 indicates the main simulations we have used to examine how important the precise eastern boundary conditions may be, and Figure 4 shows the stream functions for a selection of these numerical runs (with each flow line corresponding to 1 Sv). Cases 3 and 4 correspond to an eastern boundary divided into two subregions only for the zero or non-zero normal flux condition, but retaining one single subregion for the vorticity condition, either no-slip (Case 3) or slip (Case 4). The streamfunctions indicate that the subtropical gyre is greatly modified as compared with the standard case. The results for both cases, however, are quite unrealistic: in Case 3 all the water flows into the coastal region in a very small band close to the northern border of the basin, while in case 4 the water does not reach the central portion of the gyre. Case 6 is similar to case 5 discussed above, the only difference being that a slip rather than no-slip condition is imposed in the 10-20ºN band; the results are almost identical for both cases.

Cases 7 and 8 have the same vorticity boundary conditions as Cases 5 and 6 respectively, and the same stream function boundary conditions as in Case 9. The circulation pattern for these cases shows several small-scale loops near the coast, with water

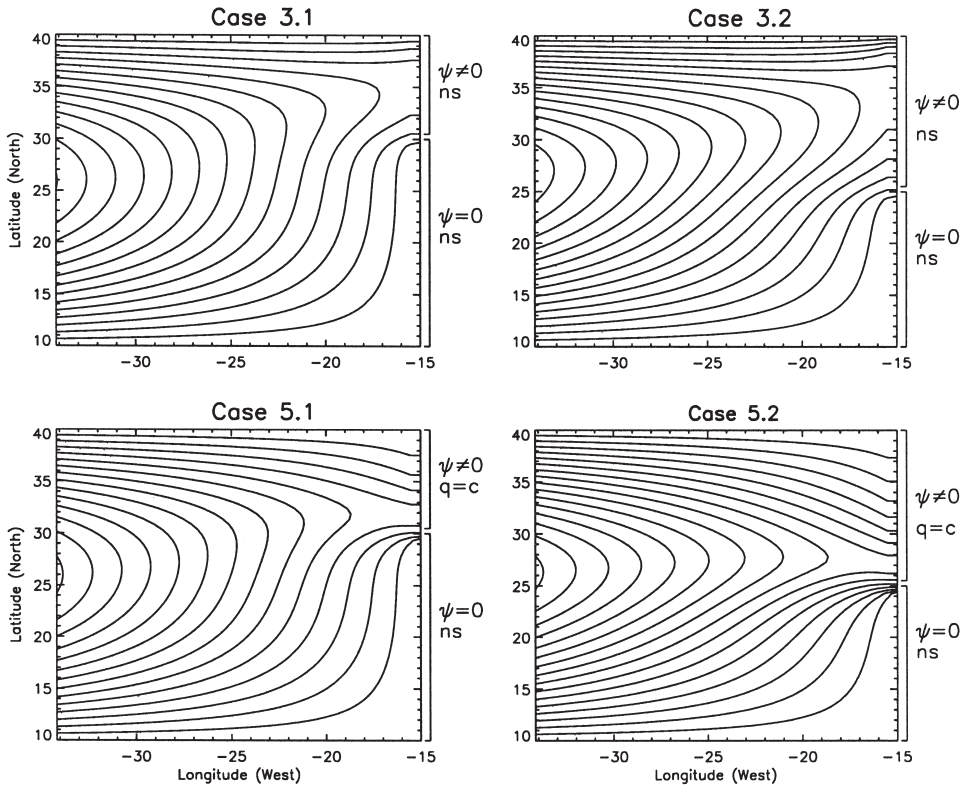


FIG. 5. – Integrated volume transport, each flow line represents 1 Sv. Case 3.1 corresponds to Case 3 with the northern subregion ranging from 30 to 40ºN. Case 3.2 corresponds to Case 3 with the northern subregion ranging from 25 to 40ºN. Case 5.1 corresponds to Case 5 with the northern subregion ranging from 30 to 40ºN. Case 5.2 corresponds to Case 5 with the northern subregion ranging from 25 to 40ºN (ns: no-slip; q = c: constant potencial vorticity; $\psi = 0$: zero normal flux; $\psi \neq 0$: non-zero normal flux).

entering and leaving the coast at several places in the 32-40ºN band. Case 10 is similar to Case 9 but with slip rather than no-slip conditions in the 10-20ºN and 27-32ºN bands, and gives very similar results. Two other possible cases (not presented here), with mixed vorticity conditions (slip and no-slip) in these bands, give almost identical results.

Cases 11 and 12 have the same vorticity boundary conditions as Cases 9 and 10 respectively, and the same stream function boundary conditions as Case 5. The results for both cases (not shown here) are totally unrealistic, with two jets of zonal flow separated by no flux in the 20-27ºN band; furthermore, Case 11 never reaches a steady-state situation. As before, mixed vorticity conditions are possible in the 10-20ºN and 27-32ºN bands, but these would not make any improvement in the results.

Figure 5 illustrates, for Cases 3 and 5, how the eastern boundary circulation pattern is modified when the meridional limits of the eastern boundary subregions are changed. The top figures correspond to Case 3 but with the upper subregion spanning from 30 to 40ºN (Case 3.1) and from 25 to 40ºN (Case 3.2). A comparison with Case 3 in Figure 4 indicates that an increase in the meridional extent of this subregion allows more water to recirculate through the coastal region. In all cases, however, this is unrealistically ejected out of the interior ocean in a very narrow area close to the northern limit of the basin. The bottom figures correspond to Case 5 but with the upper subregion spanning from 30 to 40 ºN (Case 5.1) and from 25 to 40ºN (Case 5.2). A comparison with Case 5 in Figure 4 indicates that an increase in the meridional extent of this subregion allows an increase in the amount of water that recirculates through the coastal ocean, and that this takes place in a rather smooth (and realistic) fashion.

## CONCLUSIONS

Despite the simplicity of the model, we find that the chosen specification of the eastern boundary conditions provides qualitative, and to a certain extent quantitative, features of the eastern boundary current regime which show similarities with the observations. The most coherent numerical results correspond to the case in which both non-zero normal flux and constant potential vorticity are specified simultaneously, they are rather robust and they do not depend on the choice of slip or no-slip conditions. These boundary conditions simulate the most coherent physical situation, in which southward water flow in the coastal ocean (implied by the constant potential vorticity condition) is fed smoothly through water drainage of the interior ocean. At a certain latitude the flow separates from the coast and recirculates, either locally (e.g. at 32ºN in Case 9) or definitively (e.g. at 20ºN in Case5), into the deep ocean.

## ACKNOWLEDGEMENTS

This work was supported by the European Union through project CANIGO (MAS3-CT96-0060) and the Spanish Government through projects FRENTES (AMB95-0731) and TALUD (MAR96-1893). We are thankful to G. Siedler, D. Barton, and P. Pérez for a number of useful comments and suggestions.

## REFERENCES

Arhan, M., A. Colin de Verdière and L. Mémery. – 1994. The eastern boundary of the Subtropical North Atlantic. *J. Phys. Oceanogr*. 24(6): 1295-1316.

Arakawa, A. – 1966. Computational design for long-term numerical integration of the equations of fluid motion: Two-dimensional incompressible flow. Part 1. *J. Comp. Phys*., 1, 119-143.

Asselin, R. – 1972. Frequency filters for time integration. *Month. Weath. Rev*. 100: 487-490.

Gabric, A.J., L. García, L. van Camp, L. Nykjaer, W. Eifler, and W. Schrimpf. – 1993. Offshore export of shelf production in the Cape Blanc (Mauritania) giant filament as derived from coastal zone color scanner imagery. *J. Geophys. Res*. 98: 4697-4712.

Kawase, M. and J.L. Sarmiento. – 1985. Nutrients in the Atlantic thermocline. *J. Geophys. Res*. 90: 8961-8979.

Luyten, J., J. Pedlosky, and H. Stommel. – 1983. The ventilated thermocline. *J. Phys. Oceanogr*. 13: 292-309

Pedlosky, J. – 1979. Geophysical Fluid Dynamics. Springer-Verlag, New York, 624 pp.

Pelegrí, J.L., P. Sangrà, and A. Hernández-Guerra. – 1997. Heat Gain in the Eastern North Atlantic Subtropical Gyre. *NATO ASI Series*, Vol. I, 48: 419-436.

Pelegrí, J.L., A. Marrero-Díaz, A. Antoranz, C. Gordo, A. Hernández-Guerra, A. Martínez, A. Ratsimandresy, A. Rodríguez-Santana, and P. Sangrà. – 1999. Hydrographic cruises off northwest Africa: The eastern branch of the Canary Current and the Cape Ghir filament. Proceedings of the Canigo Conference, Las Palmas de Gran Canaria, 12 to 16 September 1999.

Roache, P.J. – 1982. *Computational Fluid Dynamics*. Hermosa Publishers, 446 pp.

Schmitz, W.J. and M.S. McCartney. – 1993. On the north Atlantic circulation. *Rev. Geophys*. 31: 29-49.

Siedler, G., and R. Onken. – 1996. Eastern recirculation. In: W. Krauss (ed.), *The Warmwatersphere of the North Atlantic Ocean*, pp. 339-364. Gebruder Brontraeger, Berlin.

Stramma, L. – 1984. Geostrophic Transport in the Warm Water Sphere of the Eastern Subtropical North Atlantic. *J. Mar. Res*. 42: 537-558.

Stramma, L. and G. Siedler. – 1988. Seasonal Changes in the North Atlantic Subtropical Gyre. *J. Geophys. Res*. 93: 8111-8118.